

# Modulation of Magnetic Permeability of Ferrite Material for Electromagnetic Target Localization

Sadiq, U. A.<sup>1,2,3</sup>; Aremo, O. S.<sup>2</sup>; Oyewole E. O.<sup>2</sup>; Oluyombo, O. W.<sup>1,3</sup>

National Space Research & Development Agency, Abuja, Nigeria<sup>1</sup>; Center for Satellite Technology Development, Abuja, Nigeria<sup>2</sup>; Electrical & Electronic Engineering Dept., University of Abuja, Nigeria<sup>3</sup>;

**Abstract-** Electromagnetic target locators are important tools at checkpoints in Airports, schools, courthouses, prisons, and military installations. Electromagnetic target localization is a method of searching for electromagnetic target by employing a device that generates sound when it is in close proximity to such target. Critical parameter affecting electromagnetic target locator performances is the signal-to-noise ratio in which the signal corresponds to the target response. False alarms are caused by objects in the environment that can emit or reflect electromagnetic fields. Fluorescent lights, computer monitors, and structural steel are some examples of these objects causing interference. This research proposes the modulation of the magnetic permeability of ferrite material for detecting electromagnetic target. This was achieved by employing a ring core with highly permeable material and periodically modulates its magnetic permeability to measure the changes in the Earth's magnetic field caused by a target. In the test carried out, by modulating the magnetic permeability of ferrite material through the use of fluxgating technology, this design is able to cover a wide measurement distance while achieving high resolution and accuracy. With a 14 mm diameter MnZn Ferrite ring core material, the presence of the electromagnetic target up to 25 cm with a magnetic field and output voltage of 25  $\mu$ T and 3.459 V respectively was achieved.

## I. INTRODUCTION

Electromagnetic target locators allow the security personnel to screen individuals that may be carrying weapons or contraband that contain metallic components. Electromagnetic target locators can be walk-through or handheld models and are commonly used at checkpoints in airports, schools, courthouses, prisons, and military installations. Walk-through type can be indoor or outdoor models. The outdoor models are weatherproof and are often used at temporary venues, such as concerts or sporting events. Indoor models are typically installed at a fixed location and can however be moved if needed. Handheld types target locators are more commonly used as a secondary means of screening in conjunction with walk-through electromagnetic target locators. The handheld models are used for pinpoint screening when the alarm in the walk-through target locators have been triggered. However, they can be used as a primary screening device. Handheld target locators are weatherproof, portable, and cost less than walk-through electromagnetic target locators. A critical parameter affecting the electromagnetic target locator performances is the signal-to-noise ratio in which the signal corresponds to the target response. Further, the noise not only includes the electronic noise but also any signal produced by

the environment. Many authors have proposed methods to assess the target response but the influence of the environment on the electromagnetic target locator has received less attention (Grzegorzczak, *et al*, 2008).

This research proposes flux gating technology for electromagnetic target localization by using electromagnetic fields to passively detect the presence of electromagnetic sources. This was done by employing fluxgate sensor to measure the changes in the Earth's magnetic field caused by a target. The magnetic field measurement is achieved by gating the local magnetic field (Earth's magnetic field), by periodically modulating the magnetic permeability of a piece of ferromagnetic core material (Figure 1). The ferromagnetic core alone would act as a magnetic-flux concentrator, but combined with a drive winding to periodically drive it into magnetic saturation, thereby acts as a magnetic-flux modulator or a flux gating.

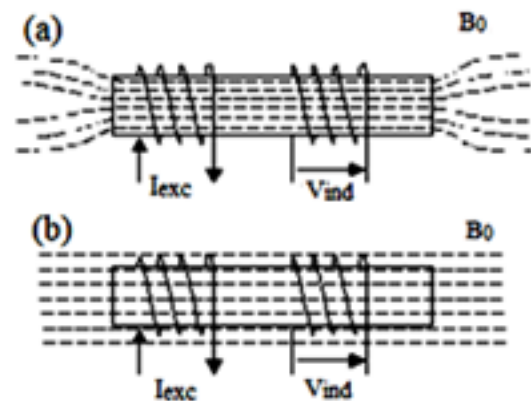


Fig.1: Fluxgate Sensor Principle, (a) Flux Recovery at High permeability (b) Flux Collapse at Low permeability (Evans, 2006).

As stated earlier, the principle of electromagnetic target locator using flux gating technology is based on the periodic saturation of a ferromagnetic core material (Zhang *et al.*, 2010; Solorzano, 2013). The permeability of the ferromagnetic material is modulated based on the  $B-H$  curve (Hysteresis loop) of the magnetic material (Suitella *et al.*, 2011), between the permeability of air and the absolute permeability of the magnetic material with a periodic excitation field at certain frequency (Ripka *et al.*, 2010; Bae *et al.*, 2013). A winding through which the excitation current is applied is placed around the core (Weiss *et al.*, 2011; Bae *et al.*, 2013). The coils are wound so that the induced excitation fields are in opposite directions (Ripka, 2001). The excitation current must be large

enough to drive the cores into saturation, typically, with currents larger in magnitude than theoretically necessary (Tumanski, 2013; Indrasari *et al.*, 2012). The output signal is obtained from the sensing coil winding that encircles the magnetic core.

Therefore, the term flux gating is clearly derived from the action of the core gating flux ‘in and out’ of the sensing coil (Butta, 2012). When the core is not saturated (with zero excitation current), the core’s relative permeability is maximum (Ripka *et al.*, 2010), which concentrates the ambient field within the core and produces a magnetic flux that is severaltimes larger than the field in a vacuum (Tumanski, 2013). During the first half cycle (with maximum excitation current), it creates magnetic field that is strong enough to saturate the core (Solorzano, 2013), which causes the permeability to become close to that of air and the field within the core collapses (Ripka, 2001). The sensor core recovers during the second half cycle of the core only to collapse again when the core saturates (Evans, 2006). The sensing coil, detects these flux changes, which occur at twice the frequency of the excitation signal, since there are two flux collapses during each cycle as clearly represented in Figure 2 (Weiss *et al.*, 2010). It can be seen that the sense voltage (Figure 2(c)) is twice the frequency of the excitation signal.

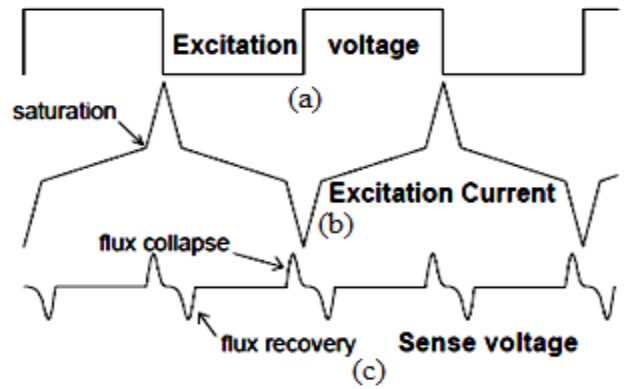


Fig.2: Fluxgate Sensor Waveform, (a) Excitation Voltage, (b) Excitation Current, and (c) Sense Voltage (Evans, 2006).

II. DESIGN PROCEDURES

The ring core material used in this research was a commercially available MnZn Ferrite material (MMG, 2014). Manganese zinc ferrite was chosen as the core material because of its high resistivity which reduces eddy current in the core, low saturation flux density, and high relative magnetic permeability. Details of the core geometric dimensions and some important parameters of the designed fluxgate sensor are shown in Table 1.

Table 1: Geometric Dimensions of the Ferrite Ring Core (Core Electronics, 2008).

Dimension	Core size
Internal radius, $d_i$ (cm)	0.8
Outer radius, $d_o$ (cm)	1.4
Height, $h_c$ (cm)	0.2
Excitation winding number (turns)	47
Sensing coil winding number (turns)	458

The geometric dimensions of the MnZn ferrite ring core are shown in Figure 3 with Radius,  $r_i$  is the internal radius of the magnetic core,  $r_o$  is the outer radius of the magnetic core, while  $h$  is the core height.

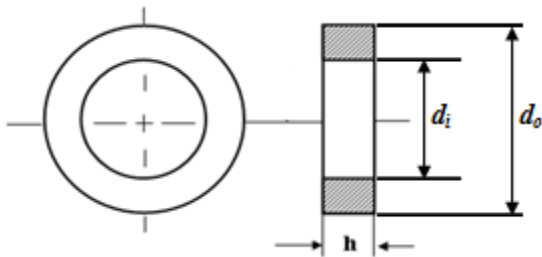


Fig.3: MnZn Ferrite Ring Core Geometric Dimensions.

The effective cross section area  $A_{core}$  of the core material was found using equation (1) (Core Electronics, 2008):

$$A_{core} = \frac{(d_o - d_i)h_c}{2} (m^2) \quad (1)$$

From the Table 2 above, the effective cross sectional area of the is calculated as:

$$A_{core} = \frac{(1.4 - 0.8) \times 0.2}{2} (cm^2)$$

Therefore, effective cross sectional area is  $A_{core} = 6 \times 10^{-6} m^2$

The effective magnetic path length  $l_{core}$  was found using equation (2) (Core Electronics, 2008):

$$l_{core} = \frac{\pi(d_o + d_i)}{2} (cm) \quad (2)$$

where, where  $d_i$  is the internal diameter of the core and  $r_o$  is the outer diameter of the core.

$$l_{core} = \frac{3.142 \times (1.4 + 0.8)}{2} (cm)$$

Therefore, effective length is

$$l_{core} = 0.034562 \text{ m}$$

Joule-heating is generated when an electric current passes through a wire conductor (Kim *et al.*, 2011). To prevent the insulation of the wire from melting, the right wire size must be considered (Kim *et al.*, 2011). By taking demagnetization factor and temperature increase of the wire into consideration, the wire diameter of 0.361mm Standard Wire Gauge (SWG 28) was chosen as the excitation coil. The inner diameter of the ring was used to determine the number of excitation coil winding as the winding turns used to be denser at the inner diameter than the outside diameter of a ring core. Therefore, the number of excitation coil turns  $N_{exc}$  was found by using equation (3):

$$N_{exc} = \frac{\pi d_i}{d_w} \quad (3)$$

where,  $d_i$  is the inner diameter of the magnetic core and  $d_w$  is the winding wire diameter.

$$N_{exc} = \frac{3.142 \times 0.008}{0.000361} \text{ turns}$$

$$N_{exc} = 69 \text{ turns}$$

The inductance  $L_{exc}$  of the excitation coil is calculated based on the magnetic permeability of 10,000 by using equation (4):

$$L_{exc} = \frac{0.4\pi\mu_c N^2 A_{core}}{l_{eff} \times 10^8} \quad (4)$$

$$\therefore L_{exc} = \frac{0.4 \times 3.142 \times 10000 \times 69^2 \times 0.06}{3.4562 \times 10^8}$$

$$\therefore L_{exc} = 10.38 \text{ mH}$$

The area of the sensing coil was calculated with a simplified formula equation (5) based on the assumption that the outside diameter and height of the ring core is equal to the length and breadth of the sensing coil respectively.

$$A_{sensing} = d_o \times \square_c \quad (5)$$

$$\therefore A_{sensing} = 0.014 \times 0.002$$

$$\therefore A_{sensing} = 2.8 \times 10^{-5} \text{ m}^2$$

The number of winding turns of the sensing coil depends on the diameter,  $d_w$ , of the wire that is used, the packing factor  $k$  ( $k \approx 0.85$  (Dehmel, 1989)) and the dimensions of the coil (Tumanski, 2011). By taking sense coil winding capacitance into consideration, the wire diameter of 0.286 mm Standard Wire Gauge (SWG 32) was chosen as the fluxgate sensing coil. The number of the sensing coil winding turns was calculated based on the assumption that the outside diameter forms the length of the winding and number of winding layers is equal to the ring core height. This is calculated as:

$$N_{sensing} = \frac{d_o \times \square_c}{d_w^2} \quad (6)$$

$$\therefore N_{sensing} = \frac{0.014 \times 0.002}{0.000286^2}$$

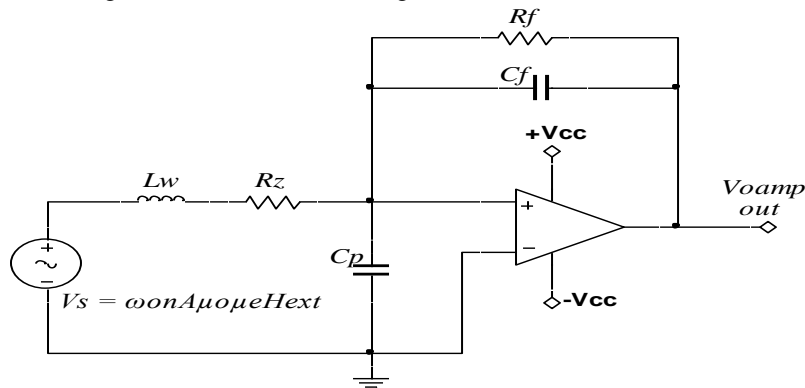
$$\therefore N_{sensing} \cong 342 \text{ turns}$$

Sensing coil inductance without the core is calculated as (Ludin, 1985; Dehmel, 1989):

$$\therefore L_{sensing} = \frac{0.85 \times 1.2568 \times 10^{-6} \times 342^2 \times (2.8 \times 10^{-5} + 30.84 \times 6 \times 10^{-6})}{0.014} \text{ H}$$

$$\therefore L_{sensing} \cong 1.9 \text{ mH}$$

The detection circuit model of sensing coil circuit is shown in Figure 4.



$$L_{air} = k \frac{\mu_0 N_{sensing}^2 A_{sensing}}{l_{sensing}} \quad (7)$$

Where:  $k$  is a magnetic field non-uniformity correction factor (also known as Nagaoka's coefficient). Nagaoka's coefficient is generally between 0.7 and 0.95 for pickup coils and always smaller than 1 (Dehmel, 1989).

$$\therefore L_{air} = \frac{0.85 \times 1.2568 \times 10^{-6} \times 342^2 \times 2.8 \times 10^{-5}}{0.014}$$

$$\therefore L_{air} \cong 0.25 \text{ mH}$$

Demagnetization factor is calculated using equation (8). Where,  $t$ ,  $d$  and  $A_{core}$  imply core thickness, average core diameter and cross sectional core area, respectively (Primdahlet al, 2002; Graef and Beleggia, 2006):

$$D_{global} = 0.223 \frac{t_{core}}{d_m} \quad (8)$$

$$\therefore D_{global} = \frac{0.223 \times 0.003}{0.011}$$

$$\therefore D_{global} \cong 6.08 \times 10^{-2}$$

When the relative permeability,  $\mu_r$  and global demagnetization,  $D_{global}$  are known, then apparent permeability,  $\mu_a$  is found as follows (Primdahl, 1979):

$$\mu_a = \frac{\mu_r}{D_{global}(\mu_r - 1) + 1} \quad (9)$$

$$\therefore \mu_a = \frac{1 \times 10^4}{6.08 \times 10^{-2} \times (1 \times 10^4 - 1) + 1}$$

$$\therefore \mu_a \cong 16.42$$

Inductance of the sensing coil with core is calculated as follows (Ludin, 1985):

$$L_{sensing} = k \frac{\mu_0 N_{sensing}^2 (A_{sensing} + 2(\mu_a - 1)A_{core})}{l_{sensing}} \quad (10)$$

Therefore, inductance of the sensing coil with core is calculated by using equation (3.14) as:

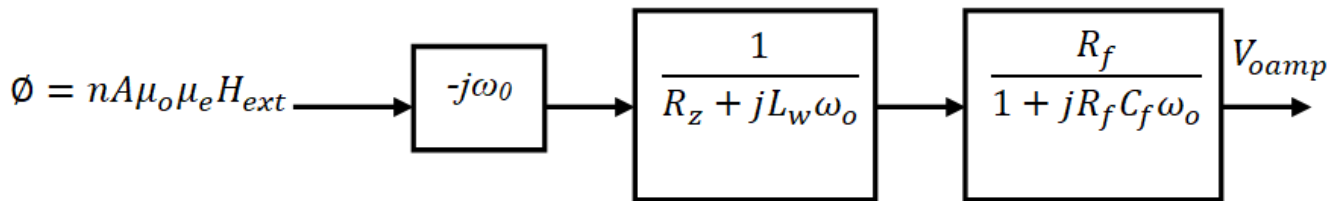


Fig.4: Circuit Model of the Detection Circuitry.

In order to calculate the performance of the designed metal detector associated with the sensing circuit, the frequency response of detection amplifier was computed as (Han *et al.*, 2012; Chen *et al.*, 2015):

$$\frac{V_{oamp}}{R_f} = \frac{V_{2f}}{R_z \left[ 1 + \left( \frac{L_w + R_f C_f}{R_z} \right) j\omega - \frac{R_f}{R_z} L_w C_f \omega^2 \right]} \quad (3.16)$$

Table 2: Optimum values of FOA Design Fluxgate Sensor

Parameters	FOA Sensor	Unit
Amplifier Feedback resistor, $R_f$	100.00	k $\Omega$
Amplifier feedback capacitor, $C_f$	150.0	nF
Amplifier input resistor, $R_z$	1.80	k $\Omega$

In order to ensure full core saturation and proper clocking of the excitation and detection circuits, the entire circuit is driven by a square wave oscillator stage at 8 kHz frequency with a duty cycle of 50%. A frequency divider stage was built, which divided the oscillator frequency by two (achieving 4 kHz). This was further divided to achieve 2 kHz driving frequency. The 2 kHz square wave signal is used to drive the excitation coil, while the 4 kHz square wave signal is used to synchronously detect the second harmonic signal from the sensing coil output.

The output currents of the frequency divider stage are weak and cannot directly drive the magnetic core to saturation. However, the sensor core requires many amperes. Hence, there is need for current amplification stage. The voltage to current converter circuit was achieved by using a low-noise class-AB power amplifier comprises of NPN and PNP transistors. The two transistors were configured as a complementary emitter-follower. The base of the two transistors was driven by the frequency divider stage which in turn provided the excitation current needed to drive the excitation coil of the proposed metal detector. At the detector stage, the output voltage from the sensing coil is very small compared to the reference voltage (2.5V – 5V) of the Analog to Digital Converter (ADC). The sensing coil of the fluxgate sensor detects the signal induced by the flux collapse (saturation) and flux recovery (de-saturation) of the core magnetizing current. This small induced voltage output signal of the sensing coil is detected and compensated by a low noise amplifier stage and filter (Figure 4). A low noise operational amplifier (OPA228) from Texas Instruments is used to design the signal conditioning stage in this research due to its ability

Where,  $R_z = R_w + R_g$ ,  $R_w$  is the pick-up coil winding resistance,  $L_w$  is the pick-up coil inductance,  $C_f$  is the amplifier feedback capacitor,  $R_f$  is the amplifier feedback resistor.

By using Firefly Optimization Algorithm (FOA), the detection amplifier circuit parameters were obtained and presented in Table 2.

to perfectly suit the system and its much smaller response time compared to the sampling period of the ADC. The frequency of the output signal of the sensing coil contains the harmonics frequency of the excitation frequency. Since the designed fluxgate sensor is expected to be capable of measuring DC magnetic field and low frequency AC magnetic field, a low pass filter was used to extract the second harmonic component from the sensing coil signal and produced a DC output voltage proportional to the Earth's magnetic field value.

### III. EXPERIMENTAL SETUP

The final dimension of the fluxgate sensor developed for the active metal detection system is 0.023 m  $\times$  0.02 m  $\times$  0.01 m as shown in Figure 5. Experimental setup for observing the excitation waveform and the modulation level of the magnetic permeability (saturation level) of the sensor core material as well as the magnetic field ground penetration depth are presented in Figure 6 and Figure 7. This was performed with the aid of Tektronix Four Channel Digital Signal Oscilloscope (model: TPS 2024B) for displaying the output waveform, Hupe Adjustable DC Power Supply (model: LN003C) for powering the sensor through the testing board and the magnetic field strength meter (Tenmars, model TM-191 portable) used for measuring the magnetic field from the magnetic field generator.



Fig.5: Complete Sensor Assembly

The modulation level of the magnetic permeability of the sensor core material through excitation and sensing coil signal waveforms were investigated by connecting the Tektronix Four Channel Digital Signal Oscilloscope (model: TPS

2024B). Figure 6 shows the output responses of the sensing coil to external magnetic field due to a bar magnet (scaled to 50µs per division on the horizontal axis and 550 mV per division on the vertical axis).

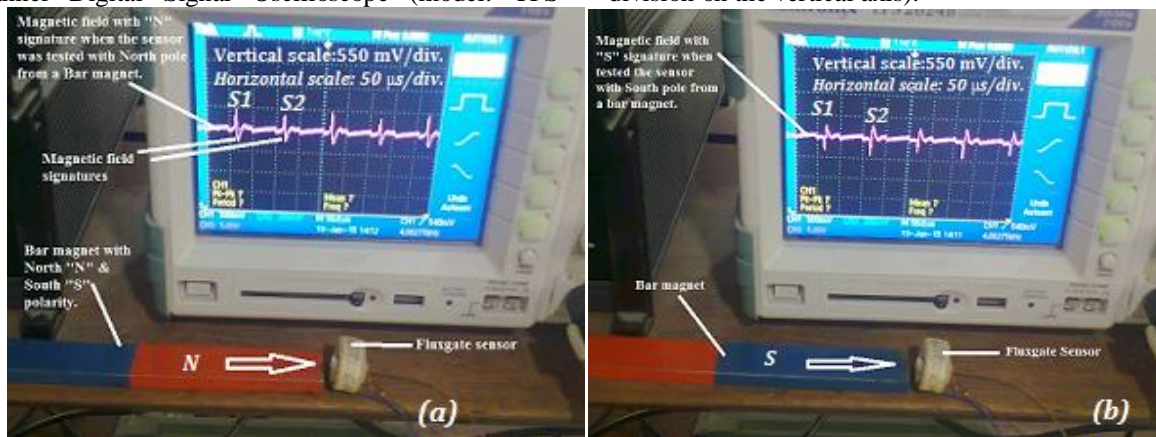


Fig.6: Experimental Setup for Magnetic Field Sensing from a Bar Magnet.

It was observed that the North-pole of a bar magnet reflects the positive external magnetic field due to the increase in the amplitude of the sensing coil output signal and the shape of the magnetic field signature. Similarly, South-pole of a bar magnet indicates the negative external magnetic field as a results of the increased amplitude of the sensing coil output

signal, but in the opposite direction with shape of the magnetic field signature. These observed changes in the amplitude and signatures of the sensing coil output signal waveform was due to the modulation of the magnetic permeability of the core material during flux gating in and out of the core material.

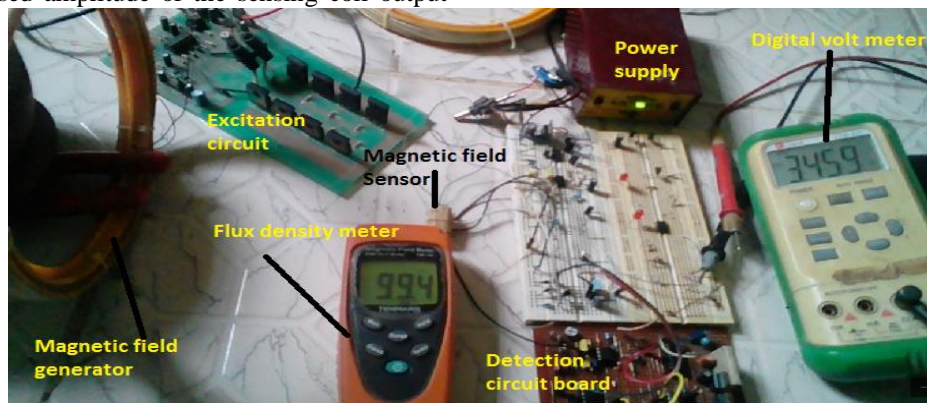


Fig.7: Experimental Setup for testing Fluxgate Sensors without Magnetic Field

As seen in Figure 7, in order to evaluate the prototype sensor with respect to the magnetic field ground penetration, a Digital Multimeter was used to measure the peak output voltages of the sensor with the corresponding external magnetic field supplied from the Helmholtz coil (used to simulate electromagnetic target). Magnetic field strength meter (calibrated magnetometer) was used to evaluate the magnitude

of the magnetic field supplied from the Helmholtz coil to the fluxgate sensors. This was done by placing the magnetic field strength meter (sensor) perpendicular to the magnetic field of the Helmholtz coil. As the sensor and magnetic field strength meter position is changing, the output voltage response to electromagnetic target were measured with respect to penetration distance and the values are presented in Table 3.

Table 3: Measured Ground Penetration Capability of the Prototype sensor

External Magnetic Field (µT)	Corresponding Voltage (V)	Penetration Distance (cm)
10.0	0.620	30.00
25.0	1.020	25.00
99.4	3.459	18.75

As shown in Table 3, from the experimental measurements, it was observed that sensor output voltage response increases with increasing magnetic field from the target. The maximum reachable distance is 30 cm with the generated minimum magnetic field of  $10\mu\text{T}$  hitting the sensor direction perpendicularly, resulting in weaker output voltage of 0.62 V, which is too small as compared to the required voltage for ADC or microcontroller interfacing. The lowest measurable distance is 18.75 cm with the maximum magnetic field value of  $99.4\mu\text{T}$  and an output voltage around 3.459 V.

#### IV. CONCLUSIONS

In this study, flux gating technology for electromagnetic target localization has been achieved by using electromagnetic fields to passively detect the presence of electromagnetic sources. The magnetic field measurement was achieved by gating the local magnetic field (Earth's magnetic field), by periodically modulating the magnetic permeability of a ferrite ring core material. Therefore, this design was able to cover a wide measurement distance while achieving high resolution and accuracy. With a 14 mm diameter MnZn Ferrite ring core material, the minimum measurable distance is 18.75 cm and the magnetic field value of  $99.4\mu\text{T}$ , resulting in stronger output voltage of 3.459 V. The maximum reachable distance is 25 cm when the maximum generated magnetic field of about  $25\mu\text{T}$  hits the sensor direction perpendicularly, resulting in weaker output voltage of about 1.0197 V. The electromagnetic target is not detectable beyond this distance due to the very weak output voltage which is not strong enough for ADC or microcontroller interfacing.

#### V. REFERENCES

- [1]. Bae, S.; Hong, Y.K.; Lee, J.; Park, J.; Jalli, J.; Abo, G.S.; Kwon, H.M. and Jayasooriya, C.K.K. (2013). Pulsed ferrite magnetic field generator for through-the-earth communication systems for disaster situation in mines. *Journal of Magnetism*, 18(1)/43-49.
- [2]. Butta, M.; Ripka, P.; Infante, G.; Badini-Confalonieri G.A., and Vázquez, M. (2010). Magnetic microwires with field induced helical anisotropy for coil-less fluxgate. *IEEE Transactions on Magnetism*, 46(7)/2562-2565.
- [3]. Chen, C.; Liu, F.; Lin, J. and Wang, Y. (2015). Investigation and optimization of the performance of an air-coil sensor with a differential structure suited to helicopter TEM exploration. *Sensors*, 25/23325-23340.
- [4]. Evans, K. (2006). Fluxgate magnetometer explained. *Invasens*, <http://www.invasens.co.uk/FluxgateExplained.PDF> Accessed 10 November 2009.
- [5]. Han, F.; Harada, S. and Sasada, I. (2012). Fluxgate and Search Coil Hybrid: A Low-Noise Wide-Band Magnetometer. *IEEE Transactions on Magnetism*, 48(11)/3700-3703.
- [6]. Indrasari, W.; Djamal, M.; Srigutomo, W. and Ramli (2012). A magnetic distance sensor with high sensitivity based on double secondary coil of fluxgate. *IOSR Journal of Applied Physics (IOSR-JAP)*, 2(5)/29-35.
- [7]. Kim, S. J.; Moon, B. Y.; Chang, Y. K. and Oh, H. S. (2011). Design of a low-cost 2-axes fluxgate magnetometer for small satellite applications. *Journal of Astronomical Space Science*, 22(1)/35-46.
- [8]. Miles, D.M.; Clurzynski, M.; Barona, D.; Narod, B. B.; Bennest, J. R.; Kale, A.; Lessard, M.; Milling, D. K.; Larson, J. and Mann, I. R. (2019). Low-noise Permalloy Ring Cores for Fluxgate Magnetometers. *Geoscience Instrumentation Methodology Data System*, 2/213-224.
- [9]. MMG (2014). Soft Ferrite Materials and Components for Power, Signal and EMC Applications. Available online at [www://adamsmagnetic.com](http://www.adamsmagnetic.com). Retrieved 25-03-2014.
- [10]. Primdahl, F. (1979). The fluxgate magnetometer. *Journal of Physics E: Science and Instrumentation*, 12/241-253.
- [11]. Ripka, P. (Ed), (2001). *Magnetic sensors and magnetometers*. Artech House, Boston, MA.
- [12]. Ripka, P.; Butta, M.; Jie, F. and Li, X. (2010). Sensitivity and noise of wire-core transverse fluxgate. *IEEE Transactions on Magnetism*, 46/654-657.
- [13]. Solorzano, E.F. (2013). A fluxgate magnetometer and an EMIS algorithm to study Europa's subsurface. *Objective Europa*, 1-9.
- [14]. Suitella, D.Y. and Windarto, D.M.T (2011). High precision fluxgate current sensor. 1-6.
- [15]. Tumanski, S. (2011). *Handbook of Magnetic Measurements* (Rev. Ed). NY: CRC press.
- [16]. Tumanski, S. (2013). Modern magnetic field sensors: A Review. *Przełqd Elektrotechniczny*, 89/1-12.
- [17]. Weiss, E. and Paperno, E. (2011). Noise investigation of the orthogonal fluxgate employing alternating direct current bias. *Journal of Applied Physics*, 109/529.
- [18]. Zhang, Y.; Steiger, M.; Hibbs, A.D.; Grimm, R.E. and Sprott, T.A. (2010). Dual-mode, fluxgate-induction sensor for UXO detection and discrimination. *Journal of Environmental Engineering and Geophysics*. 15(2)/51-64.